Modeling the Biomechanical and Injury Response of Human Liver Parenchyma under Tensile Loading

Costin D. Untaroiu, Yuan-Chiao Lu, Andrew R. Kemper

Abstract The liver is the most frequently injured abdominal organ in frontal vehicle collisions. To better predict the liver biomechanical response and injury risk during numerical simulations of traffic accidents, accurate material models of the liver should be incorporated in human finite element (FE) models. This study presents a total of 18 tension tests performed on fresh human samples of liver parenchyma at four loading rates. All these tests were simulated using specimen-specific FE models. Three different approaches were employed to identify the parameters of a first-order Ogden material model of liver parenchyma. The FE simulations with model parameters identified using an analytical approach or based on the displacement of optical markers showed a stiffer response and lower failure stress/strain than the FE-based models. These variations are probably caused by mechanical inhomogeneity of the tissue and possible violations of other assumptions employed in data analysis (e.g. constant cross-section assumption). The FE-based optimized models matched the test data well. The material models presented in this study could be easily implemented in human FE models and used to better understand the liver injury mechanism during vehicle collisions.

Keywords liver parenchyma, material properties, constitutive models, soft tissue modeling, strain-rate dependency**.**

I. INTRODUCTION

The liver is one of the most frequently injured abdominal organs in frontal vehicle crashes [1]. The liver is essential to life by regulating most chemical levels in the blood, so liver injuries associated to blunt trauma have the highest morbidity and mortality rates [2]. Capsule lacerations and parenchyma damage are common liver injuries and could be severe [3]. Therefore, accurate material and failure properties of the liver may help in designing advanced restraint systems based on computer simulations.

Several studies have investigated the failure properties of liver parenchyma in uniaxial tension using animal specimens (bovine [4-6], porcine [7-11], rabbit [12]). Recently, an extensive study presented the results of a total of 51 tension tests performed on human liver parenchyma at four loading rates [13]. The stress-strain curves until failure were obtained using high-speed video and optical markers placed on the specimens. Although these previous studies provide considerable insight into the factors that affect the tensile response of liver parenchyma, stress-strain curves obtained locally from the marker displacements are usually reported. In addition, no implementation of material test data into finite element (FE) material models and verification in terms of global properties were performed.

This study adopts an approach similar to a few recent studies [14-18], in which specimen-specific FE models were employed to identify material parameters by a FE simulation-based optimization approach. While the FE-based approach is still computationally time consuming, the material identification using an analytical-based approach was also investigated. The average stress-strain curves and failure data developed based on specimen-specific models, analytical models, and marker data were compared.

C.D. Untaroiu is a Research Associate Professor at Virginia Tech University in Blacksburg, VA (tel: +1-540-231-8997, fax: +1-540-231-8997, costin@vt.edu) . Y-C Lu, is PhD Student at Virginia Tech, A.R. Kemper is Research Assistant Professor at Virginia Tech.

II. METHODS

Experimental Testing

Uniaxial tensile tests were performed on the parenchyma of one fresh human liver. Eighteen "dog-bone shape" specimens were prepared using the custom blade assembly, slicing jig, and stamp described by Kemper et al. [13]. Prior to stamping, a template was used to position the tissue slices in order to obtain dog-bone specimens devoid of any visible deflects or vasculature. The length, width, and thickness of the gage length were approximately 55.5 mm, 10 mm and 5 mm respectively. The liver parenchyma specimens did not contain the capsule, and their longitudinal axis (loading direction) is parallel to the surface of the liver. Specimens were immersed in a bath of Dulbecco's Modified Eagle Medium (DMEM) to maintain specimen hydration until testing. It should be mentioned that one previous study [4] found no statistically significant changes in failure tensile stress or strain between specimens tested at normal room temperature (24°C) and body temperature (37°C). However, frozen storage of tissues has been shown to significantly reduce the failure tensile strain under low strain rates [5-6] and cooling storage (20 days) significantly increased the liver stiffness [19]. Therefore, the human liver was tested at a temperature close to a normal room temperature (24°C) and within 48 hours of death to minimize the effects of tissue degradation.

The testing system consisted of two motor driven linear stages (Parker Daedal MX80S, Irwin, PA) mounted to a vertically oriented aluminum plate (Fig. 1). The specimen mounting procedure described by Kemper et al. [13] was used to ensure that all specimens had a minimal but consistent preload (i.e. 1 g of tension). The specimen was aligned so that the main axis of the specimen coincided with the centerline of the load train. The testing system loaded the specimen by simultaneously moving the top and bottom grips away from one another at a constant velocity. The time histories of force measured at the load cell was inertially compensated and then fitted by a 5^{th} degree polynomial curve up to the time of failure (average R^2=0.902). The tissue failure was defined as the point of the force-time curve where the force reached a maximum and then decreased more than 3% of its peak value, and its corresponding time was defined as the "time of failure".

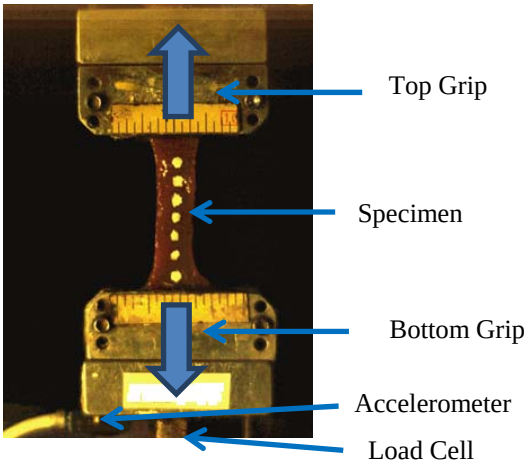

Fig. 1. Experimental setup: Human Parenchyma Tensile tests.

Prior to each test, the 3-dimensional geometry of each specimen mounted between clamps was obtained using a FARO Laser ScanArm (Laser Line Probe V3, FARO Technologies, Inc., Lake Mary, Florida) with an accuracy of ±35 µm. The specimens were scanned from different angles in order to acquire a cloud of points which can reasonably approximate the coupon surface. A poly-surface was obtained from the point cloud of each specimen using Geomagic Studio 11 (Geomagic, Inc, Morrisville, NC) which was then transformed to a Non-Uniform Rational B-Spline (NURBS) surface using Rhino vers. 5.0 (Robert McNeel & Associates, Seattle, WA).

A collinear and equidistant pattern of paint (optical) markers was applied to each specimen (Fig.1) prior to testing with 4 mm between every two markers. A high speed video camera (Phantom V4, Vision Research, Wayne, NJ) with a resolution of 7.7 pixels/mm recorded the specimen during testing (Table 1), and then a motion analysis software (TEMA Version 2.6, Linkoping, Sweden) was used to track the displacement of optical markers.

TABLE I
DATA ACQUISITION AND HIGH-SPEED VIDEO SAMPLING RATES BY LOADING RATE

Rate	Number of Samples	Desired Strain Rate (s^{-1})	Data Acquisition (kHz)	High-Speed video (Hz)
1	*5*	*0.01*	0.2	20
2	*3*	*0.1*	2	70
3	*5*	*1.0*	20	500
4	*5*	*10*	40	1000

Computational Modeling

Many studies have shown that the abdominal solid organ tissues, such as liver, can reasonably be considered isotropic and incompressible materials [20, 30, 31]. The hyperelastic formulation has been shown to be a good phenomenological constitutive approach within the nonlinear regime of biological tissues [20]. The Ogden material model showed the best matching to test data among various hyperelastic models implemented in LS-Dyna (LSTC) [21] and therefore it was chosen for parameter identification of all specimens in this study. The strain energy function of the Ogden material model [22] can be expressed as:

$$W(\lambda_1,\lambda_2,\lambda_3) = \sum_{i=1}^{N} \frac{\mu_i}{\alpha_i}\left(\lambda_1^{\alpha_i} + \lambda_2^{\alpha_i} + \lambda_3^{\alpha_i} - 3\right) \quad (1)$$

where λ_1, λ_2, λ_3 are the principal stretches, N is the order of the Ogden material model, μ_i and α_i are ith shear modulus and exponent, respectively. Three approaches were attempted in this study to identify the parameters (μ , α) of the Ogden material model [21]: 1) a *marker-based model* 2) an *analytical-based model* and 3) a *FE-based model* (Fig. 2).

1) The marker-based model

This model utilizes the constant cross-sectional area and the displacement of two markers adjacent to the failure site. The displacement between the closest optical markers adjacent to the tear location was curve fit with a 5th degree polynomial up to the time of failure (average R^2=0.999). The local stretch ratio (λ) and Green-Lagrangian (GL) strain (ε) were then calculated from the curve fit displacement data as follows:

$$\lambda = \frac{L_n}{L_0} \quad (2)$$

$$\varepsilon = \frac{1}{2}(\lambda^2 - 1) \quad (3)$$

where L_0 is the original distance between the optical markers, and L_n is the instantaneous distance between the optical markers. The 2nd Piola-Kirchhoff (PK) Stress (S) was then calculated based on the force data (Eq. 1) fitted with a 5th degree polynomial up to the time of failure (average R^2=0.902), stretch ratio and initial cross-sectional area (A_0) as follows:

$$S = \frac{F_e}{\lambda A_0} \quad (4)$$

The parameters of the Ogden first order material model (λ_1, α_1) were identified by the internal LS-Dyna optimizer based on the tensile force and local displacement (marker data) (MAT_77_O, [23]).

2) The analytical-based model

The analytical-based model approximates the specimen as a beam with an average cross-sectional area and the length between clamps. To be consistent, the cross-sectional area was calculated as the average of cross-sectional areas at three locations: the middle location and other 2 locations about 3 mm above and below the

middle location. In this approach, the strain is constant along the specimen based on the isotropy and homogenous assumptions. For an isotropic incompressible material with an applied stretch λ_1 along the loading direction, the stretches along the other directions are

$$\lambda_2 = \lambda_3 = \lambda_1^{-1/2} \tag{5}$$

The strain energy function of a first-order Ogden model, as used in the current study, is:

$$W(\lambda_1) = \frac{\mu_1}{\alpha_1}\left(\lambda_1^{\alpha_1} + 2\lambda_1^{-\alpha_1/2} - 3\right) \tag{6}$$

The nominal (first PK) stress P_1 and the second PK stress S_1 are given by:

$$P_1 = \frac{\partial W}{\partial \lambda_1} = \mu_1\left(\lambda_1^{\alpha_1 - 1} - \lambda_1^{-\alpha_1/2 - 1}\right) \tag{7}$$

$$S_1 = \frac{P_1}{\lambda_1} \tag{8}$$

and the GL strain along the elongation direction is

$$\varepsilon_1 = \frac{1}{2}(\lambda_1^2 - 1) \tag{9}$$

The stretch λ_1 can be determined from the displacement data (l_0 –initial length of specimen, $\Delta l(t)$ –the instantaneous elongation of specimen) as follows:

$$\lambda_1(t) = \frac{l_0 + \Delta l(t)}{l_0} \tag{10}$$

and the average cross-sectional area of un-deformed specimen A_0 is obtained from the reconstructed shape of specimen. Therefore, the time history of the force predicted by the model is:

$$F_m(t) = P_1(\mu_1, \alpha_1, t)A_0 \tag{11}$$

The values of material parameters (μ_1, α_1), considered as input variables, were determined by minimizing the root mean square (RMS) between the time histories of model force and the corresponding test data (Eq. 12):

$$F_{error} = \sqrt{\sum_{i=1}^{n}[F_m(t_i) - F(t_i)]^2} \tag{12}$$

where t_i is the series of *n*-time sequences equally distributed from the time when the specimen started to be loaded (time 0) up to the time of failure. An evolutionary algorithm implemented in Excel (Frontline Systems Inc., Incline Village, NV) was employed during the parameter identification process. This algorithm is a variety of genetic algorithm and local search methods, so it is appropriate for non-smooth optimization problem and global search.

3) The FE-based model

This model employs FE simulations of the specimen-specific material model using the displacement data measured at grip locations as the input. The implementation of the strain energy function for the Ogden material model in the FE software has an unconstrained form by adding a hydrostatic work term to the strain energy functional (MAT_77_O, [23]):

$$W(\lambda_1, \lambda_2, \lambda_3) = \sum_{i=1}^{N}\frac{\mu_i}{\alpha_i}(\lambda_1^{\alpha_i} + \lambda_2^{\alpha_i} + \lambda_3^{\alpha_i} - 3) + K(J - 1 - \ln J) \tag{13}$$

where K is the bulk modulus and J is the volume ratio. The liver parenchyma was assumed as a nearly incompressible material, with a Poisson's ratio of 0.4996 in all models. A tension test was simulated by prescribing the displacement-time histories, recorded during testing, to the specimen ends. In the implicit simulations (0.01 s^{-1} and 0.1 s^{-1} loading rate), a fully integrated element integration scheme was used. A constant stress element formulation with a viscosity-based hourglass control (Q_m= 0.02) was used in all explicit simulations (1 s^{-1} and 10 s^{-1} loading rates). A simulation was considered successful if the peak hourglass energy was under 3% of the peak internal energy.

As in marker-based and analytical-based models, the material parameters (μ_1, α_1), were considered as input variables, and the RMS of forces between the test data and corresponding model data was defined as the objective function to be minimized. The successive response-surface methodology (SRSM), an iterative statistical optimization method implemented in LS-Opt vers.4.2 (LSTC, Livermore, CA), was used to find a set of

parameters which minimize the objective function. A D-optimal design was used to search the test points around the optimum point determined after each iteration and a quadratic response surface was fitted through the values of objective function calculated from FE simulation [24]. The optimum point obtained using the analytical model was considered as the initial point, and the optimization process was stopped after 6 iterations. The failure GL strain was obtained from each optimized (final) simulation as the maximum GL strain along the tensile direction at the time of failure. Then, the stretch ratio and 2nd PK stress at failure were derived using failure GL strain and the parameters of the Ogden FE-based model (Eq. 7-9).

III. RESULTS

Good correlations (R^2>0.996) were observed between the force time histories of the specimen-specific models with the material parameters obtained by FE optimization and corresponding test data (Fig.2). The FE simulations with the material parameters obtained by analytical models showed consistently stiffer responses than test data, but the maximum deviation in force level was usually in a range of 5-20%. The FE simulations using the material parameters optimized from the marker model usually showed stiffer responses as well.

All specimens failed completely in the gauge length of the coupons. A failure criterion was not defined in the subject-specific FE model, but the highest values of GL strain (along the loading direction) were always observed in the gauge length (Fig. 3).

The characteristic average stress-strain curves were calculated for each loading rate and compared between three models (Fig.4). The average curves of the analytical-based model showed to be slightly stiffer than the corresponding curves of the FE-based model for all loading rates. In addition, the average stress-strain curves of the marker-based model were usually stiffer than both analytical and specimen-specific models (Fig. 4). Overall, all models showed an increase in stiffness as the loading rate increased.

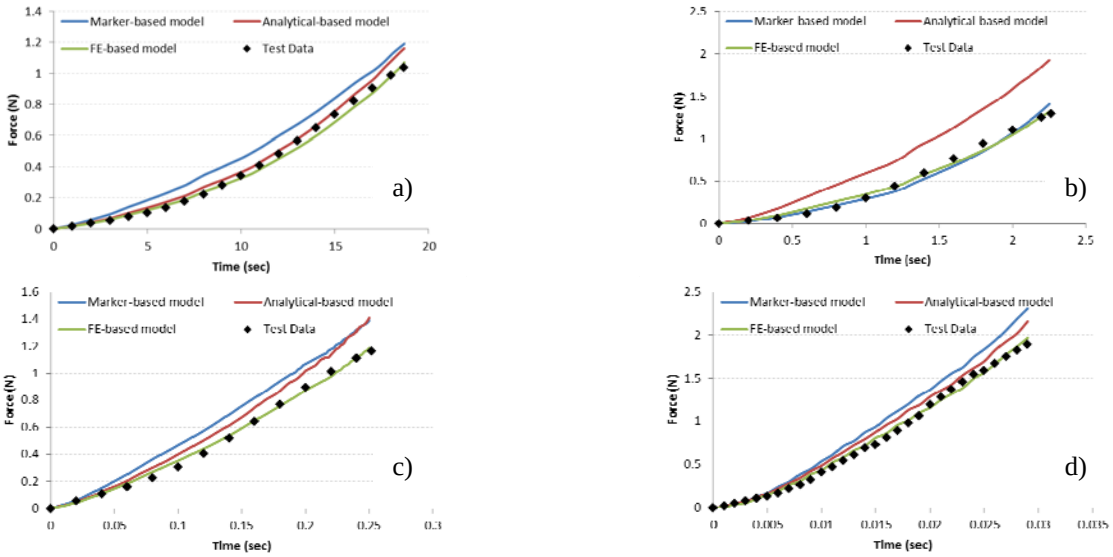

Fig. 2. Typical time histories of tensile force. Comparison between the test data and the specimen-specific FE model with various material models assigned (FE-based model. analytical-based mode, and marker-based model) for a) rate 1 b) rate 2, c) rate 3, d) rate 4

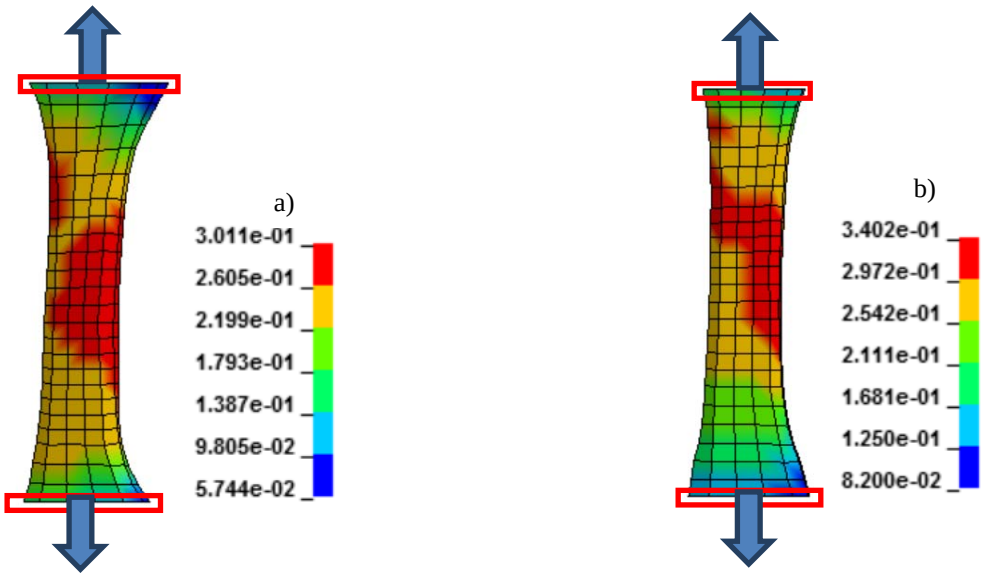

Fig.3 . The distribution of Green-Lagrangian strain before failure for typical samples at high rate tensile tests. Specimen-specific FE model with FE-based material model (a) Rate 4 (specimen H-L05-04) (b) Rate 3 (specimen H-L05-10). Red boxes represent the specimen node sets constrained to move according to the grip displacement data (boundaries conditions).

The failure values of 2nd PK stress calculated with the marker-model are close to the data reported previously [13] which used a similar (marker) approach (Fig. 5b). As in our previous study on bovine livers [21], both average failure strain and stress showed the highest values in the FE-model and the lowest in the marker-model. However, an increase in failure stress and a decrease in failure strain with the increase in loading rate were predicted by all models as reported previously [13].

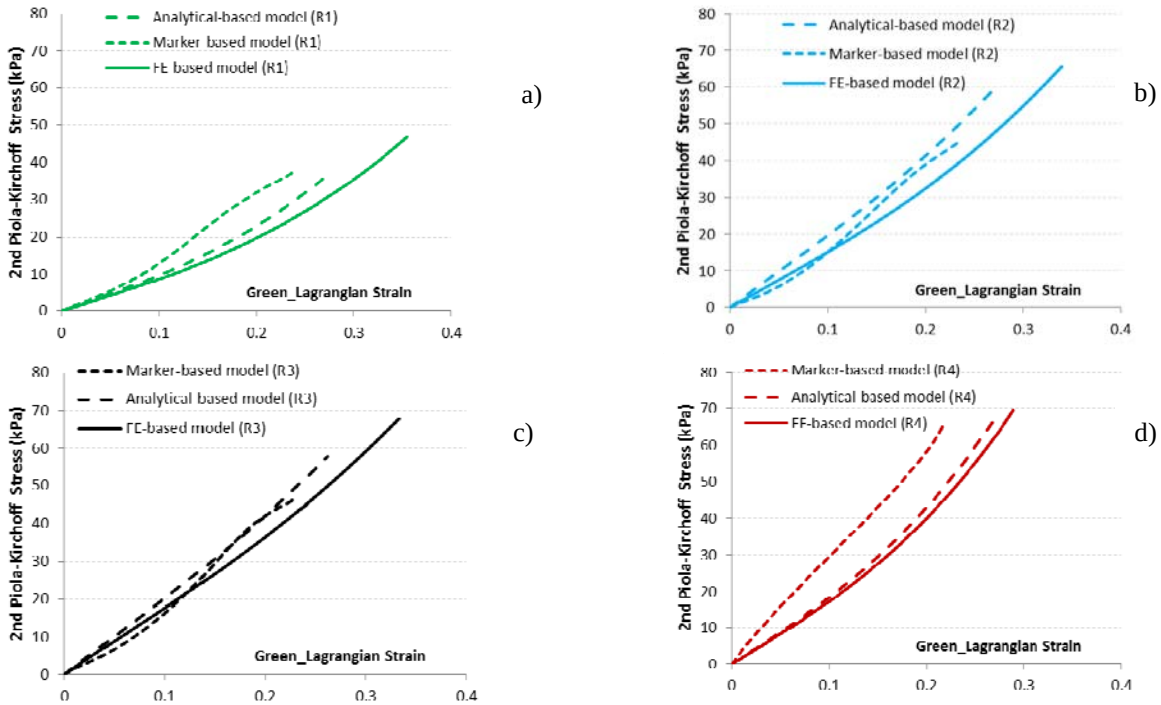

Fig. 4. The average stress-strain curves obtained using marker-based, analytical-based, and FE-based models for a) rate 1 b) rate 2, c) rate 3, d) rate 4

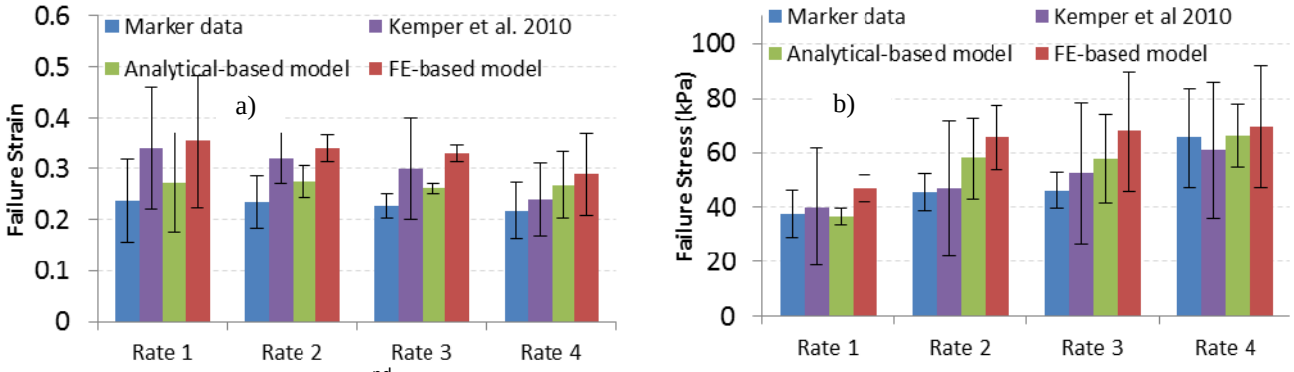

Fig.5 . Comparison of Failure 2nd Piola-Kirchhoff stress (a) and Failure Green-Lagrangian strain (b): Marker data vs. Analytical-based model vs. FE-based model.

IV. DISCUSSION

The goal of this study was to investigate rate-dependent material properties of human liver parenchyma in tension and to assess whether its behavior can be well described using a hyperelastic material model already included within commercial FE software. Uniaxial tensile tests were performed *in vitro* at four different loading rates (0.01 s^{-1}, 0.1 s^{-1}, 1 s^{-1} and 10 s^{-1}) on parenchyma samples extracted from one fresh human liver. A typical non-linear behavior was observed in the structural properties of the liver parenchyma with a convex toe region followed by an almost linear region. In addition to these regions, a concave shape close to the pre-failure region was observed especially for low rate tests (0.01 s^{-1}, 0.1 s^{-1}). A simple phenomenological model (Ogden) with only two unknown parameters showed a good overall fit to experimental data. While a better fitting to test data could be obtained in the future by increasing the complexity of the material model, a complex material model will also increase the number of unknown parameters and consequently the computational effort.

The three material models obtained using global (FE-based and analytical-based) or local (marker data) displacement data usually showed different predictions in specimen-specific FE simulations. In addition to the isotropy assumption employed by all models, each model also used additional specific assumptions. The marker-based model quantifies the behavior of tissue close to the failure site assuming a constant cross-section of the tissue between markers and a uniform deformation of the marker cross-sections during testing. It is believed that the second assumption together with some possible errors caused by video analysis (e.g. parallax errors, point tracking errors, etc.) may affect the results. The analytical approach assumes the tissue is a constant-beam which means constant stress and strain states at each time step. Since the cross-sectional area varies slightly along the middle section of the specimen and increases toward the specimen ends, the analytical-based model showed to over-predict the tensile force. The analytical approach is the cheapest in terms of computational time, so it could provide the fastest estimation. The FE-based models showed the best predictions relative to the test data. However, the FE-based models, as all other models, assume tissue isotropy and homogeneity.

A variation in stiffness and failure were observed between FE-based models corresponding to the 18 samples even though they were extracted from the same liver. While obtaining a material model which could be assigned to a liver parenchyma FE model was the main goal of these tests, employing the FE-based model and its failure parameters may be the most appropriate choice. A nearly incompressible material model of the liver parenchyma could be easily defined using MAT_181 in LS-Dyna vers. 6.0, based on the average stress-strain curves reported in this study. This Dyna material model uses a tabulated formulation of hyper-elasticity with rate effects and showed good capability in various numerical validations [25].

In addition to the isotropy and incompressibility assumptions mentioned previously, this study also has several other limitations. The Ogden model, as all other hyperelastic models, allows an unrealistic continuous increase of strain energy with the increased strain. While failure was not investigated in this study, combining the continuum damage mechanics (CDM) with the existing hyperelastic models [26] in the future may help in better prediction of pre- failure and post-failure behavior of human soft tissues. The test data provided in this study were obtained from one liver, so performing more tests on specimens obtained from different donors will provide a more accurate material characterization of human liver parenchyma.

V. CONCLUSIONS

This study presents a total of 18 uniaxial tensile tests performed at four different loading rates on fresh specimens of human liver parenchyma. In addition to the video marker-based approach used previously to quantify the stress-strain relationships, a simpler approach (analytical-based) and a more complex approach (FE-based) were employed. The FE-based approach showed the closest prediction to test data, while the other two material models usually over-predicted the response. Overall, the average stress-strain curves were close to each other except in high loading rate tests. Finally, we believe that a human FE model with accurate material and failure models would provide safety researchers with a powerful tool for better understanding the abdominal injuries [1, 27] and consequently for designing optimal restraint systems [28-29].

VI. REFERENCES

[1] Elhagediab A, Rouhana S, Patterns of Abdominal Injury in Frontal Automotive Crashes, *The 16th International Technical Conference on the Enhanced Safety of Vehicles*, 1998.
[2] Nahum, AM, Melvin J, Accidental Injury Biomechanics and Prevention (2nd Edition) *Springer*, New York, 2001.
[3] Oniscu GC, Parks RW, Garden OJ, Classification of liver and pancreatic trauma, *HPB* (Oxford), 8(1):4-9., 2006.
[4] Santago A, Kemper A, McNally C, Sparks J, Duma S, The effect of temperature on the mechanical properties of bovine liver, *Biomedical Sciences Instrumentation*, 45:376-381, 2009a.
[5] Santago A, Kemper A, McNally C, Sparks J, Duma S, Freezing affects the mechanical properties of bovine liver, *Biomedical Sciences Instrumentation*, 45: 24-29, 2009b.
[6] Lu Y-C, Kemper A.R., Untaroiu, C.D., Effect of Storage on Tensile Material Properties of Bovine Liver, 2013, submitted to publication (under review).
[7] Hollenstein M., Nava A., Valtorta D., Snedeker J., Mazza E. Mechanical Characterization of the Liver Capsule and Parenchyma. *Lecture notes in computer science*, 4072, p.150–158, 2006.
[8] Chui C, Kobayashi E, Chen X, Hisada T, Sakuma I. Transversely isotropic properties of porcine liver tissue: experiments and constitutive modelling. *Medical and Biological Engineering and Computing* 45(1):99-106, 2007.
[9] Brunon, K. Bruyère-Garnier, M. Coret Mechanical characterization of liver capsule through uniaxial quasi-static tensile tests until failure, *Journal of Biomechanics*, 43(11): 2221-2227, 2010.
[10] Sakuma I., Nishimura Y., Chui C., Kobayashi E., Inada H., Chen X., Hisada T. In vitro measurement of mechanical properties of liver tissue under compression and elongation using a new test piece holding method with surgical glue. *Lecture notes in computer science*, 2673, p.284–292, 2003.
[11] Uehara H, A study on the mechanical properties of the kidney, liver, and spleen, by means of tensile stress test with variable strain velocity, *Journal of Kyoto Prefectural University of Medicine*, 104(1):439-451, 1995.
[12] Yamada H, Strength of Biological Materials, *Williams and Wilkins*, Baltimore, 1970
[13] Kemper A, Santago A, Stitzel J, Sparks J, Duma S, Biomechanical response of human liver in tensile loading. *Annals of Advancement of Automotive Medicine*, 54:15-26, 2010.
[14] Untaroiu CD, Darvish K, Crandall J, Deng B, Wang JT, A finite element model of the lower limb for simulating pedestrian impact, *Stapp Car Crash Journal*, 49:157-181, 2005.
[15] Untaroiu CD, A numerical investigation of mid-femoral injury tolerance in axial compression and bending loading, *International Journal of Crashworthiness*, 15(1):83-92, 2010.
[16] Hu J, Klinich KD, Miller CS, Nazmi G, Pearlman MD, Schneider LW, Rupp, JD, Quantifying dynamic mechanical properties of human placenta tissue using optimization techniques with specimen-specific finite element models, *Journal of Biomechanics*, 42:2528–2534, 2009.
[17] Hu J, Klinich KD, Miller CS, Rupp JD, Nazmi G, Pearlman MD, Schneider LW, A stochastic visco-hyperelastic model of human placenta tissue for finite element crash simulations, *Annals of Biomedical Engineering*, 39(3):1074-83, 2011.
[18] Gras L-L, Mitton D, Viot P, Laporte S, Hyper-elastic properties of the human sternocleidomastoideus muscle in tension, *Journal of Mechanical Behavior of Biomedical Materials*, 15(11):131-140, 2012.

[19]Lu Y-C, Untaroiu CD, Effect of storage methods on indentation-based material properties of abdominal organs due to tissue storage methods, *Journal of Engineering in Medicine, Proc IMechE- Part H*, 227:293-301, 2012.
[20]Holzapfel GA, Nonlinear Solid Mechanics. A Continuum Approach for Engineering *Wiley*, Chichester, UK 2000.
[21]Untaroiu CD, Lu Y-C, Material characterization of liver parenchyma using specimen-specific finite element models *Journal of Mechanical Behavior of Biomedical Materials,* (in press) 2013.
[22]Ogden RW, Non-Linear Elastic Deformations, *Dover Publications*, Inc, Mineola, NY, 1997
[23]Hallquist JO, LS-DYNA keyword user's manual, Version 971. California: Livermore Software Technology Corporation, 2007.
[24]Untaroiu CD, A numerical investigation of mid-femoral injury tolerance in axial compression and bending loading, *International Journal of Crashworthiness*, 15(1):83-92, 2010.
[25]Kolling S, Du Bois PA, Benson DJ, Feng WW, A tabulated formulation of hyperelasticity with rate effects and damage, *Computational Mechanics*, 40(5):885-899, 2007.
[26]Volokh KY, On modeling failure of rubberlike materials, *Mechanics Research Communications*, 37:684-689, 2010.
[27]Untaroiu CD, Bose D, Lu Y-C, Riley P, Lessley D, Sochor M, Effect of seat belt pretensioners on human abdomen and thorax: biomechanical response and risk of injuries. *Journal of Trauma*, 72(5):1304-15, 2012.
[28]Adam T, Untaroiu C.D. Identification of Occupant Posture using a Bayesian Classification Methodology to Reduce the Risk of Injury in a Collision, *Transportation Research Part C: Emerging Technologies*, 19(6):1078-1094, 2011.
[29]Untaroiu C.D., Adam T, Performance- based Classification of Occupant Posture to Reduce the Risk, *IEEE Transactions on Intelligent Transportation Systems*, 14(2): 565-573, 2013.
[30]Pervin, F., Chen, W., and Weerasooriya, T., Dynamic compressive response of bovine liver tissues. *Journal of the Mechanical Behavior of Biological Materials*. 4(10): 76-84, 2011.
[31]Tamura, A., Omori, K., Miki, K., Lee, J., Yang, K., and King, A., Mechanical Characterization of Porcine Abdominal Organs. *Stapp Car Crash Journal*. 46: 55-69, 2002.